

Sustainable Catalysis: Rational Pd Loading on MIL-101Cr-NH₂ for More Efficient and Recyclable Suzuki–Miyaura Reactions

Vlad Pascanu,^[a, b] Qingxia Yao,^[a, c] Antonio Bermejo Gómez,^[a, b] Mikaela Gustafsson,^[a, c] Yifeng Yun,^[a, c] Wei Wan,^[a, c] Louise Samain,^[c] Xiaodong Zou,^{*[a, c]} and Belén Martín-Matute^{*[a, b]}

Abstract: Palladium nanoparticles have been immobilized into an amino-functionalized metal–organic framework (MOF), MIL-101Cr-NH₂, to form Pd@MIL-101Cr-NH₂. Four materials with different loadings of palladium have been prepared (denoted as 4-, 8-, 12-, and 16 wt % Pd@MIL-101Cr-NH₂). The effects of catalyst loading and the size and distribution of the Pd nanoparticles on the catalytic performance have been studied. The catalysts were characterized by using scanning electron microscopy (SEM), transmission electron microscopy (TEM), Fourier-transform infrared (FTIR) spectroscopy, powder X-ray diffraction (PXRD), N₂-

sorption isotherms, elemental analysis, and thermogravimetric analysis (TGA). To better characterize the palladium nanoparticles and their distribution in MIL-101Cr-NH₂, electron tomography was employed to reconstruct the 3D volume of 8 wt % Pd@MIL-101Cr-NH₂ particles. The pair distribution functions (PDFs) of the samples were extracted from total scattering experiments using high-energy X-rays (60 keV). The cata-

lytic activity of the four MOF materials with different loadings of palladium nanoparticles was studied in the Suzuki–Miyaura cross-coupling reaction. The best catalytic performance was obtained with the MOF that contained 8 wt % palladium nanoparticles. The metallic palladium nanoparticles were homogeneously distributed, with an average size of 2.6 nm. Excellent yields were obtained for a wide scope of substrates under remarkably mild conditions (water, aerobic conditions, room temperature, catalyst loading as low as 0.15 mol %). The material can be recycled at least 10 times without alteration of its catalytic properties.

Keywords: cross-coupling • heterogeneous catalysts • metal–organic frameworks • nanoparticles • palladium

Introduction

Because of increasing concern regarding environmental issues, there is a great demand for the development of efficient sustainable technologies. In the area of organic synthe-

sis, the development of efficient heterogeneous catalytic procedures^[1] has become of enormous importance, as shown by the number of reports in this field in recent years.^[2] For the industrial syntheses of building blocks and pharmaceutically relevant compounds, the elaboration of environmentally benign and cost-effective methods for carbon–carbon or carbon–heteroatom bond-forming reactions is of paramount importance. Within this family of reactions, the Suzuki–Miyaura cross-coupling reaction is one of the most robust and versatile methods for the formation of the carbon backbone of a target molecule, which is of obvious relevance for further progress in various branches of this field. A number of challenges remain to be overcome to achieve high efficiency under mild reaction conditions (e.g., ambient temperature) in environmentally friendly solvents. In addition, the use of cheaper and less-reactive substrates (e.g., aryl chlorides) also remains a challenge. Typical catalysts for these transformations can sometimes become very expensive, owing to the necessity of using transition-metal complexes in combination with different types of ligands. Thus, their high cost and environmental impact are major drawbacks for their large-scale application.^[3]

Metal–organic frameworks (MOFs), also known as coordination polymers, have gained wide interest over the last decade. They have large surface area and are highly functionalizable.^[4] MOFs have shown great potential in gas

[a] V. Pascanu, Dr. Q. Yao, Dr. A. Bermejo Gómez, Dr. M. Gustafsson, Y. Yun, Dr. W. Wan, Prof. X. Zou, Prof. B. Martín-Matute Berzelii Center EXSELENT on Porous Materials Stockholm University, SE-10691 Stockholm (Sweden) E-mail: xzou@mmk.su.se belen@organ.su.se

[b] V. Pascanu, Dr. A. Bermejo Gómez, Prof. B. Martín-Matute Department of Organic Chemistry, Arrhenius Laboratory Stockholm University, SE-10691 Stockholm (Sweden)

[c] Dr. Q. Yao, Dr. M. Gustafsson, Y. Yun, Dr. W. Wan, Dr. L. Samain, Prof. X. Zou Inorganic and Structural Chemistry Department of Materials and Environmental Chemistry Arrhenius Laboratory, Stockholm University SE-10691 Stockholm (Sweden)

Supporting information for this article is available on the WWW under <http://dx.doi.org/10.1002/chem.201302621>.

© 2013 The Authors. Published by Wiley-VCH Verlag GmbH & Co. KGaA. This is an open access article under the terms of the Creative Commons Attribution Non-Commercial NoDerivs License, which permits use and distribution in any medium, provided the original work is properly cited, the use is non-commercial and no modifications or adaptations are made.

uptake and separation,^[5] as well as in various biomedical applications,^[6] such as drug encapsulation and delivery. In addition, MOFs can be used as catalyst supports that allow for the recycling of metallic species and also prevent the contamination of the final products.^[4] However, for a MOF to be a suitable catalytic support it must be stable under the reaction conditions and allow no leaching of the active species, whilst still allowing full accessibility of the starting materials to the reaction site. However, this requirement is not always a simple task. Gratifyingly, by a thoughtful design of the linkers^[7] or subsequent postsynthetic modifications,^[8] it is possible to carefully tailor the inside of the pores so that they can better accommodate the catalyst and prevent it from leaching. One of the materials that meets all of the criteria mentioned above is MIL-101Cr [(Cr₃F(H₂O)₂O[(O₂C)-C₆H₄-(CO₂)]₃nH₂O)], which was first reported in 2005 by Férey and co-workers.^[9] MIL-101Cr has a very high specific surface area (BET, about 4100 m² g⁻¹) and contains two types of cages with diameters of 29 and 34 Å, which have pore apertures of 12 and 16 Å, respectively. MIL-101Cr is stable in water,^[10] even under very acidic conditions, and can tolerate temperatures as high as 275 °C in air. These unique features of MIL-101Cr have attracted enormous attention from researchers worldwide to explore its potential in various applications, including catalysis.^[11]

Supporting metallic nanoparticles inside a porous matrix is one of the three possible ways of exploiting MOFs in catalysis, along with supporting single-site metal complexes^[12] or by making use of the structural metal atoms in the framework as catalytically active sites.^[13,14] The main advantage of MOFs is that, by controlling the pore size, one can limit the growth of the nanoparticles, thereby obtaining small and well-distributed nanoparticles and avoiding agglomeration. This result is achieved by the infiltration of a metallic precursor into the framework, followed by subsequent reduction, thus leading to the direct formation of active nanoparticles in a controlled manner inside the pores. Recent reviews by Dhakshinamoorthy and Garcia summarized the use of metal nanoparticles that were immobilized inside MOFs as heterogeneous catalysts for various reactions, including condensation, hydrogenation, carbon-carbon coupling, and alcohol-oxidation reactions, as well as the synthesis of MeOH.^[15] Palladium nanoparticles have shown exceptional ability to catalyze a rich variety of transformations.^[16] As such, great efforts have been made to immobilize palladium nanoparticles inside the robust MIL-101Cr to form Pd@MIL-101Cr as a heterogeneous catalyst, which has been used for Suzuki coupling reactions^[17,18] or other palladium-catalyzed reactions, such as the synthesis of indoles through Sonogashira cross-coupling followed by a cycloaddition reaction,^[19] the aqueous hydrogenation of phenols into cyclohexanones,^[20] the synthesis of methyl isobutyl ketone from acetone,^[21] the hydrogenation of ketones,^[22] and even tandem processes, as cleverly illustrated by Corma and co-workers.^[23]

As a proof of concept, in 2010, Jiang and co-workers published the first report^[17] of a Suzuki coupling reaction of aryl

chlorides in water by using Pd@MIL-101Cr at 80 °C with NaOMe as a base (1.5 equiv) and tetrabutylammonium bromide (0.6 equiv) as a co-catalyst under an inert atmosphere. From this starting point, other groups have been working on the elaboration of this method to maintain high conversions whilst trying to perform the reactions under aerobic conditions at lower temperatures.^[18] Significant progress in the field of functionalized MOFs was reported in 2011 by Stock and co-workers, who described, for the first time, a rapid and facile method^[24] for the postsynthetic functionalization of MIL-101Cr by covalently grafting amino groups onto the terephthalate linkers. Bearing in mind the affinity of palladium for nitrogen atoms, this modification constituted a very important breakthrough, because it minimized the leaching of metallic species. Indeed, Cao and co-workers followed this idea and presented evidence of an increased stabilization effect of the nanoparticles in amino-functionalized MIL-53A1-NH₂ compared to MIL-53A1.^[18,25]

Over the past few years, our groups have undertaken ongoing research into the development of new and efficient transition-metal-catalyzed processes for the formation of carbon-carbon (C-C) and carbon-heteroatom (C-X) bonds^[26] and the use of MOFs in heterogeneous catalysis.^[12,14] During our investigations, we became interested in understanding the parameters that affect the efficiency of Suzuki-Miyaura cross-coupling reactions using Pd nanoparticles that are immobilized inside MIL-101Cr-NH₂. In particular, we were intrigued by the fact that the reported palladium loadings in the MOFs were often low, about 1–3 wt %, ^[16,19,21,23a,25] with only a few exceptions with higher Pd loadings (5–6 wt %).^[20] Herein, we report our investigations into the potential and limitations of MIL-101Cr-NH₂ as a catalyst support of Pd nanoparticles and its application in Suzuki-Miyaura cross-coupling reactions.^[27] We investigated how the loading of Pd into MIL-101Cr-NH₂ affected the stability of the material and its performance as a catalyst and we determined the optimal Pd loading into the framework. Moreover, the leaching of palladium under different conditions has been investigated. TEM and total scattering techniques were employed to study the Pd nanoparticles in the MIL-101Cr-NH₂ crystals. The catalyst with the optimized amount of Pd (8 wt % loaded) in MIL-101Cr-NH₂ was subjected to a systematic screening of the reaction parameters, thereby leading to efficient Suzuki-Miyaura coupling reactions, with excellent yields for a large substrate scope, including challenging heteroaromatic halides and bulky substrates, under environmentally friendly conditions (water or water/EtOH, ambient temperature, K₂CO₃). Thus, herein, we show the importance of tuning the loading of the nanoparticles in the material and of optimization of the reaction conditions for efficient and recyclable catalysis by using MOFs, which demonstrates their great potential as supports of metal nanoparticles for practical use and large-scale applications.

Results and Discussion

Synthesis and characterization of Pd@MIL-101Cr-NH₂: MIL-101Cr was synthesized according to a literature procedure.^[9] The amino functionality was introduced into MIL-101Cr in two steps, as reported by Stock and co-workers.^[24] First, nitration of the phenyl rings was achieved by the treatment of MIL-101Cr with HNO₃/H₂SO₄. In the second step, reduction of the nitro groups by using SnCl₂·2H₂O afforded Pd@MIL-101Cr-NH₂. The quantitative functionalization of MIL-101Cr was confirmed by both elemental analysis and by ¹H NMR spectroscopy after the digestion of MIL-101Cr-NO₂ and MIL-101Cr-NH₂ (see the Supporting Information, Figure S1, and the Experimental Section). Palladium loadings of 4, 8, 12, and 16 wt % were prepared by the impregnation of MIL-101Cr-NH₂ with the corresponding amount of [PdCl₂(MeCN)₂] in dry CH₂Cl₂ overnight, thus yielding Pd^{II}@MIL-101Cr-NH₂, in which Pd^{II} was coordinated to the amino groups. Subsequent reduction into Pd⁰ by using NaBH₄ afforded nanosized Pd particles inside the MIL-101Cr-NH₂ crystals, Pd⁰@MIL-101Cr-NH₂.

The synthesized material was washed with water and EtOH to eliminate all of the residues. The purity of the four final materials (4-, 8-, 12-, and 16 wt % Pd@MIL-101Cr-NH₂) was checked by energy-dispersive spectroscopy (EDS) that was connected to a SEM, elemental analysis, and by inductively coupled plasma-optical emission spectrometry (ICP-OES; Supporting Information, Table S2). The actual Pd contents, as determined by ICP-OES, for the samples of 4-, 8-, 12-, and 16 wt % Pd@MIL-101Cr-NH₂ were 4.38, 8.06, 11.29, and 15.07 wt %, respectively. Importantly, no traces of either Sn from SnCl₂ or Na from the reducing reagent were found in any of the Pd@MIL-101Cr-NH₂ samples.

The functionalization of the terephthalate linker first with nitro groups and then with amino groups was also followed by FTIR spectroscopy. The FTIR spectra and vibration frequencies of our synthesized samples, as shown in the Supporting Information, Figures S2 and S3 and Table S3, corresponded well with literature values.^[24] Strong bands at 1540 and 1357 cm⁻¹, which corresponded to N–O stretches, were observed in the spectrum of MIL-101Cr-NO₂ (Supporting Information, Figure S3). These bands disappeared after reduction of the nitro groups and a clear N–H bending frequency band at 1593 cm⁻¹ appeared instead. The C–N stretch at 1258 cm⁻¹ in MIL-101Cr-NH₂ was clearly seen in the spectrum. All of the frequency bands of the MIL-101Cr framework remained unchanged after the incorporation and reduction of palladium.

The structure of MIL-101Cr was verified by powder X-ray diffraction. The PXRD patterns of our synthesized samples of MIL-101Cr matched with those reported in the literature.^[9] The structure of MIL-101Cr remained intact after all of the postsynthetic modification steps and no obvious changes in the PXRD patterns were detected, which confirmed that MIL-101Cr-NH₂ was chemically and hydrothermally stable and that it could withstand harsh conditions, such as those applied during the nitration step (with mix-

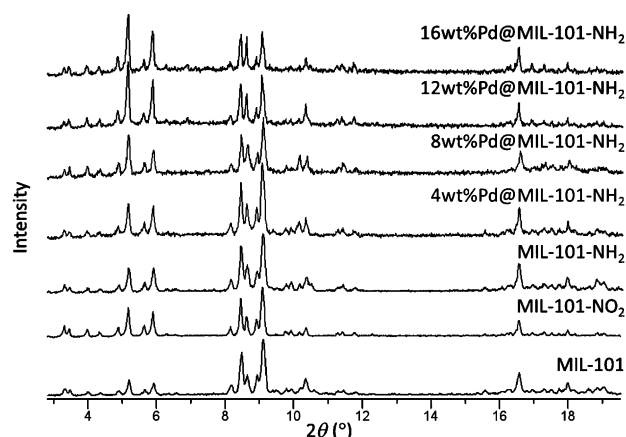


Figure 1. PXRD patterns of MIL-101Cr, MIL-101Cr-NO₂, MIL-101Cr-NH₂, and 4-, 8-, 12-, and 16 wt % Pd@MIL-101Cr-NH₂. The palladium in all four Pd-loaded samples is Pd⁰.

tures of concentrated acids) and during the reduction of Pd^{II} by using excess NaBH₄ (Figure 1). The systematic changes in the relative peak intensities in the PXRD patterns with different Pd loadings, for example, those within the regions 2θ = 5–6° and 8–9°, indicated that Pd had been incorporated into the pores of MIL-101Cr.

The weight losses of the synthesized samples upon heating in air were studied by using TGA (Supporting Information, Figure S4). MIL-101Cr was stable up to 300 °C. The thermal stability of MIL-101Cr seemed to be slightly weakened after amino-functionalization and even more so after immobilization of the Pd nanoparticles. The amount of water and solvent molecules in the pores differed between the samples, as shown by the different weight losses during heating.

N₂-sorption measurements were performed for as-synthesized MIL-101Cr, amino-functionalized MIL-101Cr-NH₂, and 4-, 8-, 12-, and 16 wt % Pd@MIL-101Cr-NH₂ samples. The N₂-adsorption isotherms, the BET surface areas, and the pore volumes are shown in Figure 2 and Table 1. The

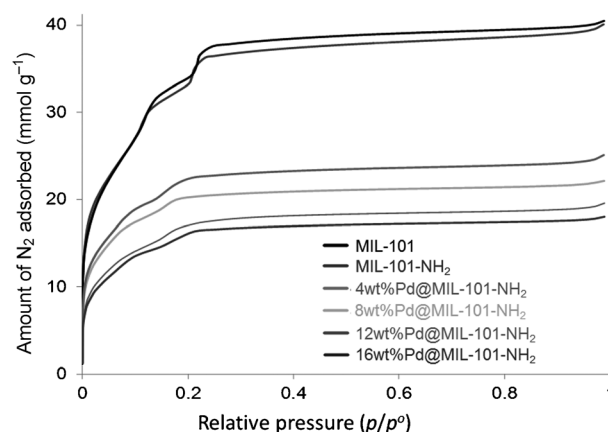


Figure 2. Nitrogen-adsorption isotherms of MIL-101Cr, MIL-101Cr-NH₂, and 4-, 8-, 12-, and 16 wt % Pd@MIL-101Cr-NH₂. The measurements were performed at 77 K.

Table 1. Specific surface areas and pore volumes of MIL-101Cr and the functionalized MIL-101Cr materials.

Material	BET surface area [m ² g ⁻¹]	Total pore volume [m ³ g ⁻¹]
MIL-101Cr	2966	1.403
MIL-101Cr-NH ₂	2869	1.389
4 wt % Pd@MIL-101Cr-NH ₂	1831	0.870
8 wt % Pd@MIL-101Cr-NH ₂	1623	0.767
12 wt % Pd@MIL-101Cr-NH ₂	1396	0.678
16 wt % Pd@MIL-101Cr-NH ₂	1321	0.625

BET surface areas of MIL-101Cr and MIL-101Cr-NH₂ are 2966 and 2869 m²g⁻¹, respectively, which are in agreement with the reported values.^[24] Compared with the parent MIL-101Cr-NH₂, the BET surface area and pore volume decreased with higher Pd loading (Table 1). The adsorption isotherms of all samples show stepwise N₂ uptake, at p/p_0 values up to 0.25, thus indicating the existence of different types of cage.

SEM analysis showed that the MIL-101Cr crystals were formed as octahedra, with sizes between 0.3 and 1.0 μm (Supporting Information, Figure S5). TEM analysis indicated that the octahedral morphology of MIL-101Cr was preserved throughout all post-modification steps, which include nitration, reduction of the nitro groups, introduction of Pd^{II}, and reduction of Pd^{II} into Pd⁰. The sizes of the Pd particles ranged from 20 to 30 Å, which were comparable to the pore diameters of unfunctionalized MIL-101Cr (29 and 34 Å, Figure 3).^[9] However, on increasing the Pd loading in MIL-101Cr-NH₂ from 11.3 to 15.1 wt%, the size of the Pd nanoparticles increased up to about 8 nm (Figure 3). These larger Pd nanoparticles were found on the surfaces of the 16 wt % Pd@MIL-101Cr-NH₂ crystals, as shown by TEM.

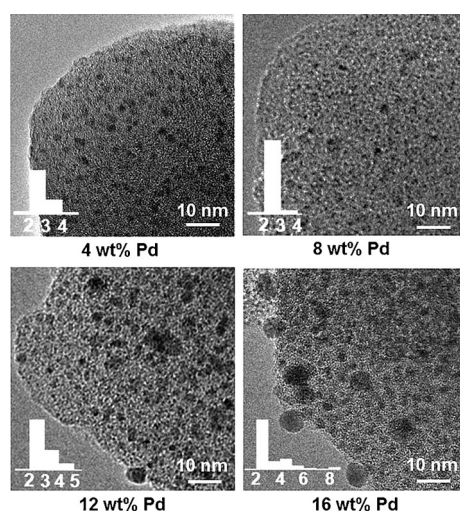


Figure 3. TEM images of samples of 4-, 8-, 12-, and 16 wt % Pd@MIL-101Cr-NH₂ with different Pd loadings (4.4, 8.1, 11.3, and 15.1 wt % Pd, respectively). Insets show the size distributions of the Pd particles as histograms, each of which was formed from about 100 Pd particles in several crystals in the TEM images. The x axis in the histograms is the size in nm and the y axis is the number of particles.

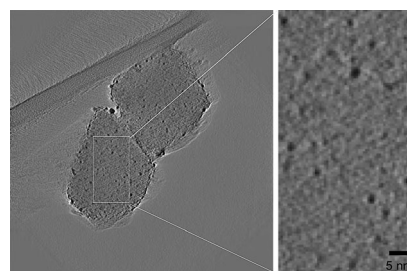


Figure 4. 2D section of the 3D tomographic image of two Pd@MIL-101Cr-NH₂ crystals with 8 wt % Pd loading, as reconstructed by the electron tomography from a tilt series of 83 TEM images with a tilt range of 41° and a tilt step of 0.5°. For the tilt series and the full tomogram, see the Supporting Information, Movies S1 and S2, respectively.

Electron tomography was performed on crystals of 8 wt % Pd@MIL-101Cr-NH₂ to study the distribution of the Pd nanoparticles. The reconstructed 3D tomographic images show that the nanoparticles are embedded inside the crystals and are homogeneously distributed throughout the crystals (Figure 4 and the Supporting Information, Movies S1 and S2). Electron diffraction and high-resolution transmission electron microscopy (HRTEM) images show that the Pd nanoparticles are crystalline (Supporting Information, Figure S6).^[28]

A better technique to study the size and distribution of the Pd nanoparticles is X-ray total scattering, because TEM only gives some local information and does not necessarily represent the nature of the bulk samples. Owing to their small particle sizes and the low concentrations of the Pd nanoparticles, no Bragg peaks for the Pd nanoparticles could be clearly seen in the PXRD patterns that were recorded on an in-house powder X-ray diffractometer. Therefore, we recorded the total scattering intensities of the 4-, 8-, 12-, and 16 wt % Pd@MIL-101Cr-NH₂ samples at the beamline P02.1, Petra III, DESY, by using a high-energy synchrotron source (60 keV). The pair distribution function (PDF), $G(r)$, was obtained by performing a Fourier transform of the total scattering intensities, including both Bragg peaks and diffuse scattering.^[29] This function describes the statistical distribution of all of the interatomic distances in a sample and, thus, is particularly suitable for investigating nanoparticles,^[30] which usually give very broadened or even no Bragg peaks by using conventional PXRD. The PDFs of the 4-, 8-, 12-, and 16 wt % Pd@MIL-101Cr-NH₂ samples were extracted from the total X-ray scattering signal truncated at a maximum Q value (Q_{\max}) of 19 Å⁻¹ (Figure 5; Supporting Information, Figure S7). For comparison, the PDFs that were calculated from the structural model of MIL-101Cr and from the structure of an ideal Pd nanoparticle (space group $Fm\bar{3}m$) with a diameter of 25 Å are also shown in Figure 5 (for the detailed procedure see the Supporting Information). The peaks in the observed PDFs of the 4-, 8-, 12-, and 16 wt % Pd@MIL-101Cr-NH₂ samples correspond to the interatomic distances in both MIL-101Cr and the Pd nanoparticle. For example, the peak at 2.0 Å corresponds to the nearest mean Cr–O distance, which is not present in the cal-

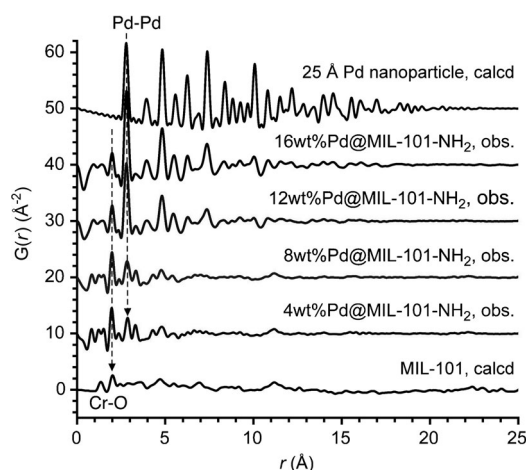


Figure 5. PDFs of samples of 4-, 8-, 12-, and 16 wt % Pd@MIL-101Cr-NH₂, compared with the calculated PDFs of MIL-101Cr (bottom) and of a Pd nanoparticle (diameter: 25 Å, top). For the sake of clarity, the PDFs are vertically stacked by 10 Å⁻².

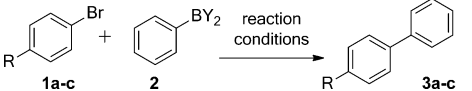
culated PDF of the pure Pd nanoparticle (Figure 5, top). The peak at 2.9 Å corresponds to the shortest distance between two Pd atoms in the Pd nanoparticle. The “ripples” on either side of the first peak in the calculated PDF of the Pd nanoparticle originate from termination effects that are due to the finite Q_{\max} of 19 Å⁻¹ that was used for the calculations and can be neglected. Whereas the peaks in the calculated PDF of the Pd nanoparticle are relatively sharp, those above 2.5 Å in the calculated PDF of MIL-101Cr are rather broad, owing to multiple overlapping of different atom–atom correlations of similar distances. The peak at 1.3 Å results from overlapping of the nearest C–C and C–O distances in MIL-101Cr. The integrated intensity of a well-defined PDF peak yields the coordination number of that specific atomic pair.^[28] For example, the integrated intensity of the first peak at 2.9 Å in the calculated PDF of the pure Pd nanoparticle will yield 12, which corresponds to the coordination number of Pd. In case of multielement samples, such as MIL-101Cr and 4-, 8-, 12-, and 16 wt % Pd@MIL-101Cr-NH₂, the peak intensities in the PDF are multiplied by a weighting factor to take into account the different scattering factors of the chemical species. Thus, in the observed PDFs of 4-, 8-, 12-, and 16 wt % Pd@MIL-101Cr-NH₂, the peak intensities can be related to the multiplicity and abundance of the atomic pairs, as well as to atomic scattering factors. By comparing the PDFs of the 4-, 8-, 12-, and 16 wt % Pd@MIL-101Cr-NH₂ samples (Figure 5), a change in the relative peak intensities can be observed; in particular, with higher Pd loading, the intensity of the peak at 2.9 Å, which corresponds to the Pd–Pd distance, increases in comparison with that of the peak at 2.0 Å, which is assigned to the Cr–O distance. This result is reasonable because, with higher Pd loading, the number of Pd atoms and, hence, the number of Pd–Pd distances of 2.9 Å is expected to increase, whereas the number of Cr–O distances of 2.0 Å in the MIL-101Cr-NH₂ should remain constant. When the PDFs of the

12- and 16 wt % Pd@MIL-101Cr-NH₂ samples are compared to the PDF of the 25 Å Pd nanoparticles (calculated), one can see that the peaks at $r > 4.5$ Å mainly originate from the Pd nanoparticles. In fact, the PDF of 16 wt % Pd@MIL-101Cr-NH₂ can be almost fully described by the structure of the Pd nanoparticles with an average size of 25 Å. The PDF of 12 wt % Pd@MIL-101Cr-NH₂ is similar to that of 16 wt % Pd@MIL-101Cr-NH₂, except that the former attenuated at a shorter distance (r). This result indicates that the size of the Pd nanoparticles in 16 wt % Pd@MIL-101Cr-NH₂ is slightly larger than that in 12 wt % Pd@MIL-101Cr-NH₂. On the other hand, the PDFs of the 4- and 8 wt % Pd@MIL-101Cr-NH₂ samples are very similar at $r > 4.5$ Å and attenuate at much larger r values compared to the PDFs of 12- and 16 wt % Pd@MIL-101Cr-NH₂. This result indicates that the sizes of the Pd particles are similar in 4- and 8 wt % Pd@MIL-101Cr-NH₂ and are smaller than those in 12- and 16 wt % Pd@MIL-101Cr-NH₂. It is worth mentioning that the PDF can also tell if there is agglomeration of the nanoparticles in the sample. Because no peaks are observed at large r values (> 20 Å), it can be concluded that there is no significant agglomeration of Pd nanoparticles in the four Pd@MIL-101Cr-NH₂ samples.

Suzuki–Miyaura cross-coupling reaction with Pd@MIL-101Cr-NH₂: In an initial series of reactions, we screened the reactivity of *p*-bromoanisole (**1a**) with different organoboron reagents and bases (Table 2). A similar screening of the reactivity of *p*-bromotoluene is shown in the Supporting Information (Table S3). Unless otherwise specified, water was used as the solvent and the reactions were performed at room temperature. Based on the characterization of the different catalysts, screening of the reaction conditions was performed with 8 wt % Pd@MIL-101Cr-NH₂ (3 mol % Pd loading). This material had small Pd nanoparticles, which ranged from 20 to 30 Å. In contrast to 12- and 16 wt % Pd@MIL-101Cr-NH₂, the 8 wt % catalyst did not show agglomeration of palladium on its surface. Moreover, 8 wt % Pd@MIL-101Cr-NH₂ contained a more favorable wt % Pd per gram of material than 4 wt % Pd@MIL-101Cr-NH₂, which is desirable from an atom-economy viewpoint. Nevertheless, the catalytic activity of all of the catalysts has been compared (see below).

Influence of the base: The nature of the base in a Suzuki–Miyaura coupling reaction greatly affects the efficiency of the reaction.^[31] In general, the reactivities of different bases in the coupling reactions of aryl iodides and bromides decreased in the order: OH⁻ > CO₃²⁻ ≫ AcO⁻. At high concentrations, bases can lead to the formation of unreactive boronates (ArB(OH)₃⁻) and, thus, the [OH⁻]/[ArB(OH)₂] ratio needs to be controlled. Moreover, the counterions can have an unexpected deceleration effect on the transmetalation step, by coordinating to the hydroxo ligand of [ArPd(OH)L₂] intermediates.^[31] With these arguments in mind, we screened a wide selection of bases and observed the stability of the 8 wt % Pd@MIL-101Cr-NH₂ catalyst, as

Table 2. Suzuki–Miyaura coupling reactions catalyzed by Pd@MIL-101Cr-NH₂; optimization of the reaction conditions.^[a]



Entry	ArBr	Boron (equiv)	Base	Solvent	<i>t</i> [h]	Yield [%] ^[b]
1	1a	PhB(OH) ₂ (2a , 1.5)	Cs ₂ CO ₃	water	6	>99
2	1a	2a (1.5)	NaOH	water	6	>99
3	1a	2a (1.5)	Na ₂ CO ₃	water	6	71
4	1a	2a (1.5)	K ₂ CO ₃	water	6	82
5	1a	2a (1.5)	BaCO ₃	water	6	94
6	1a	2a (1.5)	CsF	water	6	71
7	1a	2a (1.5)	NaOAc	water	6	– ^[c]
8	1a	2a (1.5)	<i>i</i> Pr ₂ NH	water	6	89
9	1a	2a (1.5)	<i>i</i> Pr ₂ EtN	water	6	86
10	1a	2a (1.5)	Et ₃ N	water	6	83
11	1a	2a (1.5)	C ₂ H ₄ (NH ₂) ₂	water	6	–
12	1a	2a (1.5)	No base	water	6	3
13	1b	2a (1.5)	Cs ₂ CO ₃	water	6	>99
14	1c	2a (1.5)	Cs ₂ CO ₃	water	6	84
15	1c	2a (1.5)	Cs ₂ CO ₃	water/EtOH	0.5	>99
16	1a	2a (1.2)	Cs ₂ CO ₃	water	4	68
17	1a	PhBpin (2b , 1.2)	Cs ₂ CO ₃	water	4	99
18	1a	PhBF ₃ K (2c , 1.2)	Cs ₂ CO ₃	water	4	83
19	1a	2b (1.2)	K ₂ CO ₃	water	6	>99
20	1a	2b (1.2)	K ₂ CO ₃	water	3	58
21 ^[d]	1a	2b (1.2)	K ₂ CO ₃	water	3	56
22 ^[e]	1a	2b (1.2)	K ₂ CO ₃	water	3	33
23 ^[f]	1a	2b (1.2)	K ₂ CO ₃	water	3	36

[a] Unless otherwise stated, the organoboron reagent (0.12 or 0.15 mmol), aryl halide (0.1 mmol), base (0.2 mmol), and 8 wt % Pd@MIL-101Cr-NH₂ (4 mg, 0.003 mmol, 3 mol % Pd loading) were suspended in deionized water (2 mL). The mixture was stirred vigorously at RT for 6 h in a glass vial in air (see the Supporting Information); [b] yields determined by ¹H NMR spectroscopy with 1,2,4,5-tetrachloro-3-nitrobenzene as an internal standard; [c] >95 % conversion into anisole (i.e., dehalogenation); [d] 4 wt % Pd@MIL-101Cr-NH₂ (3 mol % Pd loading); [e] 12 wt % Pd@MIL-101Cr-NH₂ (3 mol % Pd loading); [f] 16 wt % Pd@MIL-101Cr-NH₂ (3 mol % Pd loading).

shown in Table 2. When PhB(OH)₂ (**2a**) and Cs₂CO₃ were used, 4-methoxybiphenyl (**3a**) was obtained in quantitative yield within only 6 h (Table 2, entry 1). We were particularly interested in finding a less-expensive base than Cs₂CO₃ that could afford comparably high yields without harming the material. Thus, a range of other bases was tested (Table 2, entries 2–12). Sodium hydroxide also afforded excellent results (Table 2, entry 2); however, MIL-101Cr-NH₂ was not stable under these strongly basic conditions (Supporting Information, Figure S8).^[24] For this reason, carbonates were preferred because the release of hydroxy anions into the aqueous medium was slower. This property prevented the decomposition of the framework during the catalysis and also allowed for better control over the [OH[–]]/[ArB(OH)₂] ratio. Other carbonates, such as Na₂CO₃, K₂CO₃, and BaCO₃ afforded compound **3a** in 71 %, 82 %, and 94 % yield, respectively (Table 2, entries 3–5). CsF gave a comparable yield to those that were obtained with carbonates (Table 2, entry 6). Acetates have been shown to be a poor choice of base, because they lead to a slow transmetalation step.^[31] Although various amounts of the coupling product (**3a**) were detected in several experiments with NaOAc as

the base, most of the starting material underwent dehalogenation to produce anisole, which occurred faster than the coupling reaction (Table 2, entry 7). We also tested a number of organic bases (Table 2, entries 8–11) because their liquid nature may facilitate the large-scale application of this reaction. Potential problems owing to pore blocking in the case of insufficient solubility of the base would also be avoided. We found that several bases, such as *i*Pr₂NH, *i*Pr₂EtN, and Et₃N, afforded the cross-coupled product (**3a**) in very high yields (Table 2, entries 8–10). However, the stability of the nanoparticles with these bases was compromised. A comparative leaching study was performed by using one inorganic base (Cs₂CO₃) and one organic base (*i*Pr₂NH) in the coupling reaction of compound **1a** with compound **2b** in water at room temperature. After completion of the reaction (6 h), the mixture was filtered through a short pad of Celite and the Pd content in the filtrate was analyzed by ICP-OES analysis. For the reaction with Cs₂CO₃, a remarkable stability of the catalyst was observed and only 0.17 ppm Pd was detected in the filtrate. Higher Pd content was detected in the filtrate when *i*Pr₂NH was used (5.64 ppm), which, although still relatively low, was not negligible. This higher leaching was a consequence of the high affinity of palladium for nitrogenated ligands. Furthermore, if a chelating base (ethylenediamine) was used (Table 2, entry 11), all of the palladium was extracted from the support and the material lost its catalytic activity. Experiments that were performed in the absence of base showed conversions from 3 % to 21 % (Table 2, entry 12). This result may be attributed to the presence of free amino groups in the framework, which can act as basic functionalities.

Solvent and substrate polarity: Under the conditions shown in Table 2, entry 1, we compared the reactivity of compound **1a** with those of *p*-bromotoluene (**1b**) and electron-poor bromide **1c** (Table 2, entries 13 and 14). Surprisingly, in repeated experiments, the neutral (**1b**) and electron-rich substrates (**1a**) reached full conversion within 6 h, whereas the electron-poor compound **1c** was converted into the corresponding biphenyl in only 84 % yield. This unexpected reactivity, which was opposite to that in organic solvents, owing to the electronic nature of these substrates,^[32] may be attributed to the different solubilities of compounds **1a–1c** in water. Indeed, when water was replaced by a mixture of EtOH and water (1:1, in which differences in solubility were minimized), bromide **1c** afforded the corresponding coupling product in excellent yield within only 30 min (Table 2, entry 15).

Organoboron reagents: Next, we evaluated other organoboron derivatives. To clearly observe any differences in their reactivities, the reactions were stopped after only 4 h and only

1.2 equivalents of the organoboron reagents were used (Table 2, entries 16–18). Pinacol phenylboronate (**2b**) afforded the highest yield, followed by phenyltrifluoroborate potassium salt (**2c**) and phenylboronic acid (**2a**). The lower reactivity of compound **2a** can be explained by its preference to form boroxine trimers, which are inactive under these mild reaction conditions.^[33] Thus, we decided to continue our investigation by using pinacolate ester **2b**. Furthermore, the use of compound **2b** compensated for the loss of reactivity that was observed when Cs₂CO₃ was replaced by K₂CO₃ and quantitative yields could be obtained with the latter base by using only 1.2 equivalents of PhBpin (Table 2, entry 19).

Comparison of Pd@MIL-101Cr-NH₂ catalysts with different Pd loadings: With the optimized conditions in hand, we compared the activities of the 4-, 8-, 12-, and 16 wt % Pd@MIL-101Cr-NH₂ catalysts (Table 2, entries 20–23). The reactions were analyzed before full conversion had occurred (3 h) by using a Pd loading of 3 mol %. Whereas the reactions with 4- and 8 wt % Pd@MIL-101Cr-NH₂ afforded very similar and satisfactory yields (Table 2, entries 20 and 21), the reactions with 12- and 16 wt % Pd@MIL-101Cr-NH₂ afforded significantly lower yields (Table 2, entries 22 and 23). This behavior was in agreement with the TEM and PDF analyses, which showed that the nanoparticles in the 12- and 16 wt % Pd@MIL-101Cr-NH₂ catalysts were larger with broader size distributions. The poorer performance of the MOFs with higher Pd loadings may be explained by an increased difficulty in the diffusion of the substrates and the products through these materials, owing to pore blocking.

Leaching tests: The stability and performance of the immobilized nanoparticles were evaluated according to the approach reported by Sheldon et al.^[34] A hot-filtration test was performed by stirring the 8 wt % Pd@MIL-101Cr-NH₂ catalyst in boiling water for 15 min, followed by filtration through a pad of Celite. The filtrate was subsequently used as the solvent for the reaction of compound **1a** with compound **2a** under similar reaction conditions to those in Table 2, entry 1, but in the absence of the palladium catalyst. After 6 h, only 3% conversion was detected by ¹H NMR spectroscopy. The Pd leached into solution after catalysis when carbonates were used as the base was only 0.17 ppm (see above). Together with the high recyclability of the catalyst (see below), these results clearly demonstrate the stability of the Pd nanoparticles in MIL-101Cr-NH₂.

Substrate scope: Based on this series of observations (Table 2), we screened a variety of substrates with 8 wt % Pd@MIL-101Cr-NH₂ as the catalyst (3 mol % Pd loading) and K₂CO₃ as the base, because K₂CO₃ is environmentally benign and about 20-times cheaper than Cs₂CO₃. Moreover, potassium has been shown to be the counteraction that infers the least-intense decelerating effect in the transmetalation step.^[31] These results are shown in Table 3. The reactions were either performed in water or in water/EtOH

mixtures (1:1 v/v). Aryl bromides **1a–1c** were easily coupled within short reaction times (6 h in water, 30 min in water/EtOH) at room temperature (Table 3, entries 1–3). 2-Bromonaphthalene (**1d**), which showed very low solubility in water at ambient temperatures, afforded compound **3d** in only 22% yield. However, 97% yield was obtained after only 2 h in water/EtOH, in which the solubility of the substrate was increased (Table 3, entry 4). Interestingly, the reaction of 9-bromoanthracene (**1e**) proceeded very slowly, even in water/EtOH after a prolonged reaction time (Table 3, entry 5). This result may be due to the large size of this substrate, which results in limited access to 8 wt % Pd@MIL-101Cr-NH₂, and the catalysis mainly occurred at the Pd nanoparticles on the external surfaces of the MOF catalyst particles. Importantly, heteroaromatic substrates **1f** and **1g** could also be coupled in high yields (Table 3, entries 6–7). However, a lower yield was obtained for 2-bromopyridine (**1h**; Table 3, entry 8). Slightly higher leaching of palladium was observed for substrates that contained heteroatoms: 3.10 ppm Pd was found in the filtrate after the reaction of bromopyridine (**1g**), whereas only 0.17 ppm was found after the coupling of compound **1a** (see above). The coupling reactions of aryl chlorides required more elevated temperatures, which, disappointingly, were more favorable for the formation of byproducts (that is, dehalogenation (ArH) or homocoupling (Ar–Ar) products). Activated aryl chlorides **1i** and **1j** successfully reacted in water and they returned good-to-excellent yields with little or no formation of undesired byproducts (Table 3, entries 9 and 10). However, if EtOH was used as a co-solvent, both activated and inactivated substrates **1j–1m** returned very good conversions but only fair yields, with the concomitant formation of significant amounts of homocoupling and dehalogenation products (Table 3, entries 10–13).

Recycling tests: The recyclability of 8 wt % Pd@MIL-101Cr-NH₂ was investigated in the reaction of *p*-bromotoluene. The experiments were performed on a larger scale (1 mmol) than in previous investigations to facilitate separation and minimize handling errors. After each run, the solid catalyst was separated by centrifugation, washed with water and EtOH (twice each), dried under vacuum, and reused. As shown in Figure 6, the catalyst remained highly active, even after 10 cycles.^[35] Interestingly, the PXRD pattern after the tenth cycle was different from that of MIL-101Cr-NH₂, but similar to that of another phase, presumably MIL-88B-NH₂ (Supporting Information, Figure S9).^[36] This phase-transformation phenomenon is currently under investigation in our laboratories. TEM analysis showed the presence of some limited aggregation of Pd nanoparticles on the surfaces of the MOF catalysts after the 10th cycle (Supporting Information, Figure S10). Because the size of the nanoparticles remained unchanged, the aggregation did not seem to significantly affect the efficiency of the catalyst. Elemental analysis of the recycled 8 wt % Pd@MIL-101Cr-NH₂ material showed an overall loss of 0.96 wt % Pd after 10 runs. Yields of between 97% and >99% were obtained in the recycling

Table 3. Suzuki coupling reactions of various aryl bromides and chlorides catalyzed by 8wt% Pd@MIL-101Cr-NH₂.^[a]

Entry	Substrate	Product	Yield (water, 6 h) [%] ^[b]	Yield (water/EtOH, 0.5 h) [%] ^[b]
1			> 99 (94)	95
2			> 99 (96)	> 99
3			84	99 (96)
4			22	97 (94) ^[c]
5			0	19 ^[d]
6			99 (89)	–
7			99 (92)	–
8			47	95 (90)
9			99 (95) ^[e]	–
10			70 (62) ^[f,e]	54 ^[g,e]
11			52 (47) ^[h,e]	50 ^[i,e]
12			4 ^[j,e]	44 ^[k,e]
13			3 ^[l,e]	36 ^[m,e]

[a] Unless otherwise stated, the pinacol phenylboronate (0.12 mmol), aryl halide (0.1 mmol), K₂CO₃ (0.2 mmol), and 8 wt% Pd@MIL-101Cr-NH₂ (4 mg, 0.003 mmol, 3 mol% Pd loading) were suspended in either deionized water (2 mL) or water/EtOH (1:1). Then, the mixture was stirred vigorously at RT in air for 6 h (water) or 30 min (water/EtOH) in a glass vial (see the Supporting Information); [b] yield determined by ¹H NMR spectroscopy with 1,2,4,5-tetrachloro-3-nitrobenzene as an internal standard; yield of the isolated product is given in parentheses; [c] 2 h; [d] 16 h; [e] 80 °C; [f] 96% conversion, 13% homocoupling; [g] 89% conversion, 9% homocoupling, 16% dehalogenation; [h] 68% conversion, 13% homocoupling; [i] 89% conversion, 12% homocoupling, 15% dehalogenation; [j] 98% conversion; toluene was the main byproduct; [k] 100% conversion, 12% homocoupling, 32% dehalogenation; [l] 44% conversion; anisole was the main byproduct; [m] 79% conversion, 10% homocoupling, 23% dehalogenation.

runs. Based on these excellent results, we decreased the Pd loading by 20 times to 0.15 mol% and performed the reactions on the same scale and under similar conditions to those in Table 2, entry 19, and the reaction proceeded to completion within 4 h. This result indicates that Pd@MIL-101Cr-NH₂ is a highly efficient catalyst.

Conclusion

In summary, we have provided evidence for a strong relationship between the amount of palladium that is loaded into MIL-101Cr-NH₂ and the catalytic properties of the corresponding system. The MIL-101Cr-NH₂ material was found to be an excellent support for palladium nanoparticles. The size, distribution, and reactivity of palladium nanoparticles were shown to be influenced by the amount of palladium metal that was impregnated into the framework. The nanoparticles were investigated by using both conventional and advanced methods, such as electron tomography and PDF analysis. The best performance was observed for MIL-101Cr-NH₂ that contained about 8 wt% palladium nanoparticles. This result indicates that an optimal ratio was achieved between the amount of loaded catalyst and the number of pores that remained accessible for the diffusion of the substrates and the products. The catalyst 8 wt% Pd@MIL-101Cr-NH₂ displayed remarkable activity in the Suzuki–Miyaura cross-coupling reaction. Aryl and heteroaryl bromides and activated aryl chlorides were successfully coupled within short reaction times under mild conditions

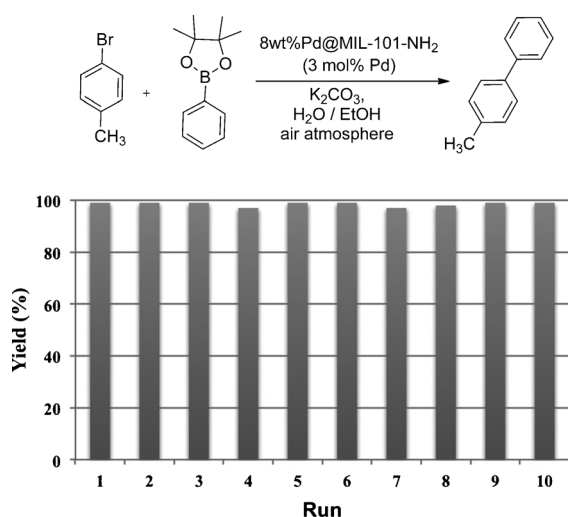


Figure 6. Recycling experiments on a 1 mmol scale; reaction time of each run: 0.5 h.

(ambient temperature and 80 °C, respectively) in benign solvents (water and EtOH). Our investigations have also shown that the solubility and hydrophobicity of the substrates significantly affect their ability to access the catalyst pores in water, but this limitation is minimized by employing EtOH as a co-solvent. The excellent recyclability of the 8 wt % Pd@MIL-101Cr-NH₂ catalyst makes it a promising candidate for large-scale Suzuki–Miyaura cross-coupling reactions. This thorough study of the structural and catalytic properties of metallic nanoparticles that are supported on a MOF material can stand as a model for detailed investigations of other related heterogeneous systems, in search for a better understanding of the underlying mechanism of heterogeneous catalysis with MOFs.

Experimental Section

General: All chemicals and solvents were used as received without further purification. Powder X-ray diffraction (PXRD) was performed in the Bragg–Brentano geometry on a PANalytical X'Pert PRO diffractometer that was equipped with a Pixel detector and Cu_{Kα1} radiation ($\lambda = 1.5406 \text{ \AA}$). The samples were dispersed over zero-background Si plates. SEM and energy-dispersive spectroscopy (EDS) were performed on a JEOL-7000F field-emission scanning electron microscope operating at 12 kV. The samples were precoated with a thin carbon film. The presence of possible byproducts was investigated by using EDS. TEM observations were performed on a JEOL TEM (JEM-2100F) operating at 200 kV. The MIL-101Cr samples were dispersed in absolute EtOH and then treated by ultrasonication for 2 min. A droplet of the suspension was transferred onto a copper grid and dried in air. A tilt series of TEM images for electron tomography was recorded with a tilt step of 0.5° and an angular range of 41° (83 images in total). TomoJ^[37,38] was employed for the tomographic reconstruction. The images were aligned by using the Pd particles themselves as markers. Ten iterations of the ART^[39] algorithm were performed in TomoJ with a relaxation coefficient of 0.1. ImageJ^[40] was used to preprocess the tilt series of TEM images. Thermogravimetric analysis (TGA) was performed under a flow of air between 20 and 500 °C with a heating rate of 2 °C min⁻¹ on a thermogravimetric analyzer (PERKIN

ELMER TGA 7) that was equipped with a platinum pan. N₂-adsorption isotherms were recorded at 77 K on a Micromeritics ASAP2020 analyzer. The samples for N₂ adsorption were first exchanged with absolute EtOH before activation. The samples were degassed by heating at 120 °C overnight prior to the sorption measurements. Specific surface areas were calculated from the data in the adsorption branch at $p/p_0 = 0.05\text{--}0.30$. The total pore volume was calculated from the uptake at $p/p_0 = 0.99$. FTIR spectroscopy was performed on a Varian 670-IR spectrometer. Elemental analysis was performed on a Carlo Erba Flash 1112 elemental analyzer and the Cr and Pd contents were determined by inductively coupled plasma-optical emission spectrometry (ICP-OES) on a Varian Vista MPX ICP-OES at Medac Ltd, Chobham, UK. High-energy X-ray diffraction experiments were carried out at a fixed energy of approximately 60 keV at a wavelength of 0.2073 Å (determined by using a CeO₂ standard) at the beamline P02.1 of Petra III, Desy, Hamburg. The 2D diffraction images were integrated into a linear scattering signal by using the Fit2D software.^[41] The pair distribution function (PDF), $G(r)$, was obtained by sine Fourier transform of the normalized scattering intensity to a maximum Q value, $Q_{\text{max}} = 19 \text{ \AA}^{-1}$, by using the PDFgetX2 software.^[42] The PDF of the Pd nanoparticles was calculated with the PDFgui software^[43] (for a detailed procedure, see the Supporting Information). ¹H NMR spectra were recorded at 400 MHz; ¹³C NMR spectra were recorded at 100 MHz on a Bruker Avance spectrometer. ¹H and ¹³C NMR chemical shifts (δ) are reported in ppm relative to tetramethylsilane, with the solvent resonance as an internal standard (CDCl₃: $\delta_{\text{H}} = 7.26$ ppm, $\delta_{\text{C}} = 77.16$ ppm; [D₆]DMSO: $\delta_{\text{H}} = 2.50$ ppm, $\delta_{\text{C}} = 39.5$ ppm). Coupling constants (J) are given in Hz. High-resolution mass spectra (HRMS) were recorded on a Bruker microTOF ESI-TOF mass spectrometer.

Synthesis of Pd@MIL-101Cr-NH₂: Samples of MIL-101Cr (Cr₃F-(H₂O)₂O[(CO₂)-C₆H₄-(CO₂)₃·*n*H₂O])^[9,44] MIL-101Cr-NO₂ (Cr₃(H₂O)₂O-[(CO₂)-C₆H₃NO₂-(CO₂)₃·*n*H₂O])^[24] and MIL-101Cr-NH₂ (Cr₃(H₂O)₂O-[(CO₂)-C₆H₃NH₂-(CO₂)₃·*n*H₂O])^[24] were prepared according to literature procedures. Samples of Pd@MIL-101Cr-NH₂ with four different loadings of Pd nanoparticles that were intended to be 4, 8, 12, and 16 wt % Pd were prepared by using analogous procedures, as given below.

Synthesis of MIL-101Cr-NH₂-PdCl₂: For MIL-101Cr-NH₂-PdCl₂ affording 8 wt % Pd@MIL-101Cr-NH₂, the following procedure was used: A mixture of MIL-101Cr-NH₂ (0.240 g, 3.15×10^{-4} mol), [PdCl₂(MeCN)₂] (0.055 g, 2.11×10^{-4} mmol), and anhydrous CH₂Cl₂ (30 mL) was stirred overnight at RT (18 h). The solid was obtained by centrifugation, washed with anhydrous CH₂Cl₂ (2 × 10 mL), and dried at 40 °C for 2 h under vacuum. To obtain samples with 4, 12, and 16 wt % Pd loading, the amount of [PdCl₂(MeCN)₂] that was used to afford 8 wt % Pd loading was multiplied by 0.5, 2, and 3, respectively; the amount of solvent was kept the same.

Synthesis of 8 wt % Pd@MIL-101Cr-NH₂: NaBH₄ (0.076 g, 2 mmol) was added portion-wise to a mixture of MIL-101Cr-NH₂-PdCl₂ (0.140 g) and EtOH (30 mL) at 0 °C. The green mixture became darker after about 2 min. The reaction was stirred for an additional 2 h at 0 °C to complete the reduction. The solid was obtained by centrifugation, washed twice with water (45 mL) and once with EtOH (45 mL), and the dark-green solid was dried at 85 °C overnight (18 h) in air.

Digestion of MIL-101Cr: In a typical experiment, the material (10 mg) was suspended in an aqueous solution of NaOH (2.0 M, 1 mL) and ultrasonicated for 30 min. The water was evaporated under vacuum and the residue was analyzed by ¹H NMR spectroscopy in deuterated DMSO (Supporting Information, Figure S1).

General procedure for the Suzuki–Miyaura cross-coupling reactions: Unless otherwise stated, pinacol phenylboronate (24.5 mg, 0.12 mmol), the aryl bromide (0.1 mmol), K₂CO₃ (27.6 mg, 0.2 mmol), and 8 wt % Pd@MIL-101Cr-NH₂ (4 mg, 0.003 mmol) were suspended in deionized water (2 mL) and the mixture was stirred vigorously at RT for 6 h. Then, the mixture was extracted into CH₂Cl₂ (4 mL), the organic phase was separated, the volatile compounds were evaporated, and the residue was analyzed by ¹H NMR spectroscopy. To isolate the final product, the reaction was repeated on a larger scale (×4) and the crude reaction mixture was purified by column chromatography on silica gel (pentane or pentane/EtOAc mixtures).

Acknowledgements

This project was supported by the Knut and Alice Wallenberg Foundation, the Swedish Research Council (VR), the Swedish Governmental Agency for Innovation Systems (VINNOVA) through the Berzelii Center EXSELENT, and the Knut and Alice Wallenberg Foundation. B.M.-M. was supported by VINNOVA through a VINNMER grant. W.W. was supported by a postdoctoral grant from the Carl-Trygger Foundation. L.S. was supported by The Consortium for Crystal Chemistry (C³), Röntgen-Ångström Cluster. The electron microscopy facility was supported by the Knut and Alice Wallenberg Foundation. The authors acknowledge Petra III, Desy, for the use of the synchrotron facility (I-20120456 EC) and Dr. Jozef Bednarcik for his assistance in using the Beamline P02.1.

- [1] a) M. Zhang, J. Guan, B. Zhang, D. Su, C. Williams, C. Liang, *Catal. Lett.* **2012**, *142*, 313–318; b) M. M. Dell'Anna, M. Mali, P. Mastrorilli, A. Rizzuti, C. Ponzoni, C. Leonelli, *J. Mol. Catal. A* **2013**, *366*, 186–194; c) B. J. Borah, D. K. Dutta, *J. Mol. Catal. A* **2013**, *366*, 202–209; d) A. Kumbhar, S. Jadhav, S. Kamble, G. Rashinkar, R. Salunkhe, *Tetrahedron Lett.* **2013**, *54*, 1331–1337.
- [2] a) K. Sawai, R. Tatumi, T. Nakahodo, H. Fujihara, *Angew. Chem.* **2008**, *120*, 7023–7025; *Angew. Chem. Int. Ed.* **2008**, *47*, 6917–6919; b) N. Zhang, D. J. Hoffman, N. Gutsche, J. Gupta, V. Percec, *J. Org. Chem.* **2012**, *77*, 5956–5964; c) B. H. Lipshutz, S. Ghorai, *Aldrichimica Acta* **2012**, *45*, 3–16; d) U. Yilmaz, S. Deniz, H. Kucukbay, N. Sireci, *Molecules* **2013**, *18*, 3712–3724.
- [3] a) For a review, see: J. Magano, J. R. Dunetz, *Chem. Rev.* **2011**, *111*, 2177–2250; b) N. Marion, P. de Frémont, I. M. Pujik, E. C. Ecarnot, D. Amoroso, A. Bell, S. P. Nolan, *Adv. Synth. Catal.* **2007**, *349*, 2380–2384; c) C. Boos, D. M. Bowles, C. Cai, A. Casimiro-Garcia, X. Chen, C. A. Hulford, S. M. Jennings, E. J. Kiser, D. W. Piotrowski, M. Sammons, R. A. Wade, *Tetrahedron Lett.* **2011**, *52*, 7025–7029.
- [4] For a special issues on metal–organic frameworks, see: *Acc. Chem. Res.* **2005**, *38*, 215; *J. Solid State Chem.* **2005**, *178*, 2409; *Chem. Soc. Rev.* **2009**, *38*, 1201; *Chem. Rev.* **2012**, *112*, 673.
- [5] a) For reviews, see: H.-L. Jiang, Q. Xu, *Chem. Commun.* **2011**, *47*, 3351–3370; b) M. C. Das, S. Xiang, Z. Zhang, B. Chen, *Angew. Chem.* **2011**, *123*, 10696–10707; *Angew. Chem. Int. Ed.* **2011**, *50*, 10510–10520. J.-R. Li, J. Sculley, H.-C. Zhou, *Chem. Rev.* **2012**, *112*, 869–932.
- [6] For a review, see: P. Horcajada, R. Gref, T. Baati, P. K. Allan, G. Maurin, P. Couvreur, G. Férey, R. E. Morris, C. Serre, *Chem. Rev.* **2012**, *112*, 1232–1268.
- [7] For a review, see: F. A. Almeida Paz, J. Klinowski, S. M. F. Vilela, J. P. C. Tomé, J. A. S. Cavaleiro, J. Rocha, *Chem. Soc. Rev.* **2012**, *41*, 1088–1110.
- [8] For a review, see: K. K. Tanabe, S. M. Cohen, *Chem. Soc. Rev.* **2011**, *40*, 498–519.
- [9] G. Férey, C. Mellot-Draznieks, C. Serre, F. Millange, J. Dutour, S. Surblé, I. Margiolaki, *Science* **2005**, *309*, 2040–2042.
- [10] a) J. Ehrenmann, S. K. Henninger, C. Janiak, *Eur. J. Inorg. Chem.* **2011**, 471–474; b) A. Khutia, H. U. Rammelberg, T. Schmidt, S. Henninger, C. Janiak, *Chem. Mater.* **2013**, *25*, 790–798.
- [11] a) Y. K. Hwang, D.-Y. Hong, J.-S. Chang, S. H. Jung, Y.-K. Seo, J. Kim, A. Vimont, M. Daturi, C. Serre, G. Férey, *Angew. Chem.* **2008**, *120*, 4212–4216; *Angew. Chem. Int. Ed.* **2008**, *47*, 4144–4148; b) A. Henschel, K. Gedrich, R. Kraehnert, S. Kaskel, *Chem. Commun.* **2008**, *44*, 4192–4194; c) N. Maksimchuk, K. A. Kovalenko, V. P. Fedin, O. Kholdeeva, *Chem. Commun.* **2012**, *48*, 6812–6814; d) L. Bromberg, Y. Diao, H. Wu, S. A. Speakman, T. A. Hatton, *Chem. Mater.* **2012**, *24*, 1664–1675.
- [12] F. Carson, S. Agrawal, M. Gustafsson, A. Bartoszewicz, F. Moraga, X. Zou, B. Martín-Matute, *Chem. Eur. J.* **2012**, *18*, 15337–15344.
- [13] A. Dhakshinamoorthy, M. Alvaro, H. Chevreau, P. Horcajada, T. Devic, C. Serre, H. Garcia, *Catal. Sci. Technol.* **2012**, *2*, 324–330.
- [14] a) M. Gustafsson, A. Bartoszewicz, B. Martín-Matute, J. Sun, J. Grins, T. Zhao, Z. Li, G. Zhu, X. Zou, *Chem. Mater.* **2010**, *22*, 3316–3322; for a related heterogeneous catalyst, see: b) T. Yang, A. Bartoszewicz, J. Ju, J. Sun, Z. Liu, X. Zou, Y. Wang, G. Li, F. Liao, B. Martín-Matute, J. Lin, *Angew. Chem.* **2011**, *123*, 12763–12766; *Angew. Chem. Int. Ed.* **2011**, *50*, 12555–12558.
- [15] For reviews, see: a) A. Dhakshinamoorthy, H. Garcia, *Chem. Soc. Rev.* **2012**, *41*, 5262–5284; b) A. Dhakshinamoorthy, M. Opanasenko, J. Čejka, H. Garcia, *Catal. Sci. Technol.* **2013**, *3*, 2509–2540.
- [16] For a review, see: K. C. Nicolaou, P. G. Bulger, D. Sarlah, *Angew. Chem.* **2005**, *117*, 4516–4563; *Angew. Chem. Int. Ed.* **2005**, *44*, 4442–4489.
- [17] B. Yuan, Y. Pan, Y. Li, B. Yin, H. Jiang, *Angew. Chem.* **2010**, *122*, 4148–4152; *Angew. Chem. Int. Ed.* **2010**, *49*, 4054–4058.
- [18] Y. Huang, Z. Zheng, T. Liu, J. Lu, Z. Lin, H. Li, R. Cao, *Catal. Commun.* **2011**, *14*, 27–31.
- [19] H. Li, Z. Zhu, F. Zhang, S. Xie, H. Li, P. Li, X. Zhou, *ACS Catal.* **2011**, *1*, 1604–1612.
- [20] H. Liu, Y. Li, R. Luque, H. Jiang, *Adv. Synth. Catal.* **2011**, *353*, 3107–3113.
- [21] Y. Pan, B. Yuan, Y. Li, D. He, *Chem. Commun.* **2010**, *46*, 2280–2282.
- [22] J. Hermannsdörfer, R. Kempe, *Chem. Eur. J.* **2011**, *17*, 8071–8077.
- [23] a) F. G. Cirujano, F. X. Llabrés i Xamena, A. Corma, *Dalton Trans.* **2012**, *41*, 4249–4254; b) A. Arnanz, M. Pintado-Sierra, A. Corma, M. Iglesias, F. Sánchez, *Adv. Synth. Catal.* **2012**, *354*, 1347–1355.
- [24] S. Bernat, V. Guillerme, C. Serre, N. Stock, *Chem. Commun.* **2011**, *47*, 2838–2840.
- [25] Y. Huang, S. Liu, Z. Lin, W. Li, X. Li, R. Cao, *J. Catal.* **2012**, *292*, 111–117.
- [26] a) A. Bartoszewicz, M. Livendahl, B. Martín-Matute, *Chem. Eur. J.* **2008**, *14*, 10547; b) N. Ahlsten, B. Martín-Matute, *Chem. Commun.* **2011**, *47*, 8331; c) I. Cumpstey, S. Agrawal, K. E. Borbas, B. Martín-Matute, *Chem. Commun.* **2011**, *47*, 7827–7829; d) A. Bartoszewicz, R. Marcos, S. Sahoo, A. K. Inge, X. Zou, B. Martín-Matute, *Chem. Eur. J.* **2012**, *18*, 14510–14519; e) N. Ahlsten, A. Bermejo Gómez, B. Martín-Matute, *Angew. Chem.* **2013**, *125*, 6393–6396; *Angew. Chem. Int. Ed.* **2013**, *52*, 6273–6276.
- [27] For a brief comparison of the performances of several recently reported heterogeneous nanopalladium catalysts, see the Supporting Information, Table S1, and: a) O. Verho, A. Nagendiran, E. V. Johnston, C.-w. Tai, J.-E. Bäckvall, *ChemCatChem* **2013**, *5*, 612–618; b) N. Shang, C. Feng, H. Zhang, S. Gao, R. Tang, C. Wang, Z. Wang, *Catal. Commun.* **2013**, *40*, 111–115; c) K. Karami, M. Ghasemi, N. H. Naeini, *Catal. Commun.* **2013**, *38*, 10–15; d) L. Isfahani, I. Mohammadpoor-Baltork, V. Mirkhani, A. R. Khosropour, M. Moghadam, S. Tangestaninejad, R. Kia, *Adv. Synth. Catal.* **2013**, *355*, 957–972.
- [28] a) W. Lu, B. Wang, K. Wang, X. Wang, J. G. Hou, *Langmuir* **2003**, *19*, 5887–5891; b) F. Wang, C. Li, L.-D. Sun, C.-H. Xu, J. Wang, J. C. Yu, C.-H. Yan, *Angew. Chem.* **2012**, *124*, 4956–4960; *Angew. Chem. Int. Ed.* **2012**, *51*, 4872–4876.
- [29] T. Egami, S. J. L. Billinge, *Underneath the Bragg Peaks: Structural Analysis of Complex Materials* (Ed: R. W. Cahn), Pergamon, Oxford, **2003**.
- [30] a) S. J. L. Billinge, *J. Solid State Chem.* **2008**, *181*, 1695–1703; b) K. Page, T. Proffen, H. Terrones, M. Terrones, L. Lee, Y. Yang, S. Stemmer, R. Seshadri, A. K. Cheetham, *Chem. Phys. Lett.* **2004**, *393*, 385–388.
- [31] C. Amatore, A. Jutand, G. Le Duc, *Chem. Eur. J.* **2012**, *18*, 6616–6625.
- [32] a) E. P. Urriolabeitia, in *Oxidative Addition and Transmetalation–Palladacycles: Synthesis Characterization and Applications* (Eds: J. Dupont, M. Pfeffer), Wiley-VCH, Weinheim, **2008**, pp. 35–67; b) K. C. Lam, T. B. Marder, Z. Lin, *Organometallics* **2007**, *26*, 758–760.
- [33] A. Scrivanti, V. Beghetto, M. Bertoldini, U. Matteoli, *Eur. J. Org. Chem.* **2012**, 264–268.

- [34] R. A. Sheldon, M. Wallau, I. W. C. E. Arends, U. Schuchardt, *Acc. Chem. Res.* **1998**, *31*, 485–493.
- [35] For critical reviews on the nature of the active species with heterogeneous Pd catalysts, see: a) N. T. S. Phan, M. V. D. Sluys, C. W. Jones, *Adv. Synth. Catal.* **2006**, *348*, 609–679; b) M. Pagliaro, V. Pandarus, R. Ciriminna, F. Béland, P. D. Carà, *ChemCatChem* **2012**, *4*, 432–445.
- [36] S. Surblé, C. Serre, C. Mellot-Draznieks, F. Millangea, G. Férey, *Chem. Commun.* **2006**, 284–286.
- [37] C. Messaoudi, T. Boudier, C. O. Sanchez Sorzano, S. Marco, *BMC Biochem.* **2007**, *8*, 288.
- [38] C. O. Sorzano, C. Messaoudi, M. Eibauer, J. R. Bilbao-Castro, R. Hegerl, S. Nickell, S. Marco, J. M. Carazo, *BMC Biochem.* **2009**, *10*, 124.
- [39] G. T. Herman, A. Lent, S. W. Rowland, *J. Theor. Biol.* **1973**, *42*, 1–32.
- [40] W. S. Rasband, ImageJ, US National Institute of Health, Bethesda, MD, <http://imagej.nih.gov/ij/>, **1997–2012**.
- [41] A. P. Hammersley, S. O. Svensson, M. Hanfland, A. N. Fitch, D. Hausermann, *J. High Pressure Res.* **1996**, *14*, 235–248.
- [42] X. Qiu, J. W. Thompson, S. J. L. Billinge, *J. Appl. Crystallogr.* **2004**, *37*, 678–678.
- [43] C. L. Farrow, P. Juhas, J. W. Liu, D. Bryndin, E. S. Božin, J. Bloch, T. Proffen, S. J. L. Billinge, *J. Phys. Condens. Matter* **2007**, *19*, 335219.
- [44] Y. Huang, Z. Lin, R. Cao, *Chem. Eur. J.* **2011**, *17*, 12706–12712.

Received: July 5, 2013
Published online: November 21, 2013